Chapter 3

Transparent Conducting Thin Film Preparation of Carbon Nanotube

Xiaogang Sun, Jie Wang, Wei Chen, Xu Li, Manyuan Cai, Long Chen, Zhiwen Qiu, Yapan Huang, Chengcheng Wei, Hao Hu and Guodong Liang

Additional information is available at the end of the chapter

http://dx.doi.org/10.5772/intechopen.79164

Abstract

Transparent conducting films have a wide range of applications in the fields of flat panel displays, solar cells, and touch panels for their both good conductivity and light transmittance. Carbon nanotubes (CNTs) transparent conducting film has become a potential alternative for next-generation transparent conducting film systems owing to high conductivity, light transmittance and flexibility. The multiwalled carbon nanotubes (MWCNTs) conductive liquid was prepared by dispersing MWCNTs in alcohol through ultrasonic and high-speed shearing process with an addition of carbon nanotube alcohol dispersant (TNADIS) as the dispersant. The transparent conducting film was fabricated on polyethylene terephthalate (PET) transparent film by spin-coating process. The film was used as interlayer between the electrode and the separator to improve electrochemical performance of lithium-sulfur (Li-S) batteries.

Keywords: multiwalled carbon nanotubes, transparent conducting film, lithium-sulfur batteries, transmittance

1. Introduction

Carbon nanotubes have been the hotpot of scientific research ever since their discovery. Due to their unique structure, carbon nanotubes (CNTs) have shown outstanding performance in electromagnetics, mechanics, heat and optics [1–5], which have made them attractive in lithium ion batteries, supercapacitors, composite materials and many other aspects [2–6]. At present, carbon

nanotubes have been produced in large scale. However, the carbon nanotubes entangled with each other and shown severe agglomeration effect [7, 8]. The carbon nanotubes are nanoscale materials and the specific surface area is large, the surface energy is high, and there is a great Van der Waals force between the carbon nanotubes [9–15]. In addition, the carbon nanotubes exhibited a structure of one-dimensional tubular and the aspect ratio is relatively large, they have similar interlocking characteristics to fibers, which result in easy agglomeration of carbon nanotubes. In order to solve the technical problem and obtain a stable carbon nanotube dispersion, many dispersion methods are introduced to prepare the dispersion liquid of the carbon nanotube. Physical dispersion methods include grinding, ball milling, ultrasonic, and high-speed shear. The chemical dispersion methods include strong acid and alkali treatment and the addition of dispersant [16–18]. Each dispersion method has its own advantages but all have some drawbacks that make it difficult to produce a very stable dispersion of carbon nanotubes.

Transparent conductive films are widely used in the fields of flat panel displays, solar cells, touch panels owing to good electrical conductivity and light transmission. Currently, many transparent conductive films are studied: metal film, n-type transparent conductive oxide film, p-type transparent conductive oxide film, special film system (TiN conductive film, etc.) and multilayer film system. Carbon nanotubes (CNTs) have also become the focus of research due to their good properties in conductivity, light transmission and flexibility. Therefore, the CNTs transparent conducting films have also become the focus of research. The dispersibility of carbon nanotubes has an important influence on the quality of the film of the conductivity as well as transparency. In this chapter, MWCNTs ethanol conductive liquid was prepared by ultrasonic vibration and high-speed shearing process. The MWCNTs transparent conductive film was prepared by spin-coating.

The high theoretical capacity of 1675 mAh/g and high energy density of 2600 Wh/kg, lithium–sulfur (Li-S) batteries have become the most promising alternatives for next-generation electrochemical energy storage systems [19–22]. In addition, abundant resources, low cost and ecofriendliness of sulfur make Li-S batteries have higher commercial value [23–25]. However, the actual capacity of the current lithium-sulfur battery is greatly lower than the theoretical capacity and the cycle life is poor, which seriously hampered the practical application of lithium-sulfur battery [26]. The main reason is that the diffusion and dissolution of intermediate lithium polysulfides during cycling (Li_2S_n, $4 \leq n \leq 8$) which led to notorious shuttle effects. This resulted in high self-discharge, active material loss and low Coulombic efficiency [27–31]. In this work, we report multiwalled carbon nanotubes paper (MWCNTsP) as a current collector, MWCNTs transparent conductive film was used as the interlayer between the positive electrode and the separator [32, 33]. The new structure of Li-S battery retarded the dissolution and dispersion of lithium polysulfides (LPSs). The Li-S batteries with MWCNTs transparent conductive film showed high discharge capacity, excellent cycle stability and high sulfur loading.

2. Fabrication and characterization of MWCNTs

MWCNTs were synthesized by chemical vapor deposition with benzene being used as carbon feedstock, ferrocene as a catalyst precursor, thiophene as growth promotion agent, and

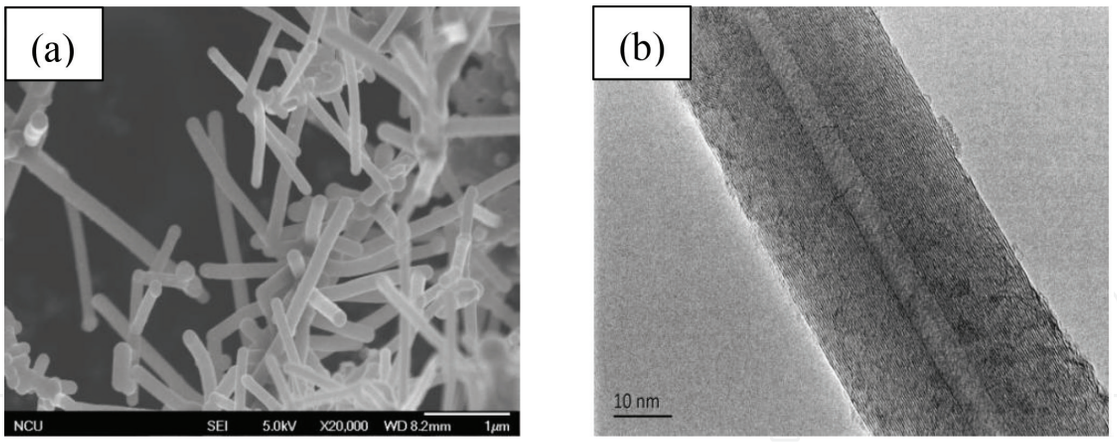

Figure 1. (a) SEM and (b) TEM images of MWCNT.

hydrogen as carrier gas. The reaction temperature was around 1200°C. The raw MWCNTs were treated at a high temperature of 3000°C for graphitization.

The SEM image of multiwalled carbon nanotube was shown in **Figure 1(a)**, it was observed that the MWCNTs have a one-dimensional tubular structure and are not entangled with each other. This suggested that the line MWCNTs can be easily dispersed in various matrix. The MWCNTs have also excellent mechanical and physicochemical properties. The TEM (**Figure 1(b)**) image shows that MWCNTs have one-dimensional tubular structure and the carbon atoms are arranged in a regular and orderly manner.

3. MWCNTs transparent conducting film

3.1. Experiment

3.1.1. Preparation of MWCNTs conductive liquid

The raw multiwalled carbon nanotubes (R-MWCNTs) and graphitized multiwalled carbon nanotubes (G-MWCNTs) were, respectively, ball-milled in a ball mill for 2 h. The TNADIS dispersant was dissolved in anhydrous ethanol and its mass concentration was 0, 0.025, 0.05, 0.1, 0.2, 0.4, 0.6, 0.8, and 1%, respectively. Then, two types of MWCNTs were, respectively, added to the above solution with a concentration of 1 wt.%. The dispersion liquid of MWCNTs was prepared by ultrasonically dispersing for 30 min and high-speed shearing for 1 h. The R-MWCHTs are marked as 1#-8# and the G-MWCNTs are marked as 9–16#.

3.1.2. Performance testing

Raman spectroscopic analysis, transmission electron microscopy (TEM) and scanning electron microscopy (SEM) were used to analyze and observe the morphology and structure of MWCNTs. The optimal addition ratio of dispersant was determined by measuring the precipitation after centrifugation. In addition, the stability of the conductive liquid was observed and analyzed. The stability of the conductive liquid of MWCNTs was characterized by detecting the Tyndall effect after the conductive liquid was left standing for 5 months.

3.2. Results and discussion

3.2.1. Raman spectroscopy and TEM, SEM analysis

The Raman spectra of MWCNTs was shown in **Figure 2**, it can be used to analyze the crystallinity of MWCNTs. The relative intensity of D and G peaks (IG/ID) can reflect the degree of crystallization of MWCNTs samples. G-MWCNTs have a much higher IG/ID of 4.16 than R-MWCNTs (IG/ID = 0.67). The G peak at 1585 cm^{-1} is called the tangential stretching mode of the MWCNTs, which is a reflection of the degree of order, and similar peaks are observed in the graphite. The D peak at 1334 cm^{-1} is a reflection of the defect and disorder degree in the MWCNTs, and the D peak of the MWCNTs originates from the structural defects of the carbon nanotubes. Both the D peak after graphitization and the 2D peak at 2656 cm^{-1} were observed due to the double resonance process of the two resonant electron states of the MWCNTs.

The TEM image of raw MWCNTs was shown in **Figure 3(a)**, and it was observed that the arrangement of carbon atoms on the surface of R-MWCNTs is disordered. It indicated there are a lot of amorphous carbons and defects on surface of R-MWCNTs. After MWCNTs were graphitized at 3000°C, the carbon atoms shown a regular and orderly manner (**Figure 3(b)**).The G-MWCNTs have a high degree of crystallinity which is consistent with the results obtained by Raman spectroscopy. **Figure 2(c)** and **(d)** shows the SEM images before and after graphitization of MWCNTs, respectively. It can be seen that the MWCNTs used in the experiment are linear whisker carbon nanotubes. However, G-MWCNTs and R-MWCNTs are agglomerated before being dispersed due to van der Waals forces. From the SEM images, it can be seen that the graphitized carbon nanotubes have less impurities and higher purity.

3.2.2. Effect of dispersant TNADIS content on dispersion of MWCNTs

The precipitation mass versus dispersant content was exhibited (**Figure 4**), which depicts a linear reduce with increasing dispersant content until the minimum precipitation mass is achieved. Hereafter the sediment increased with increasing dispersant. The minimum

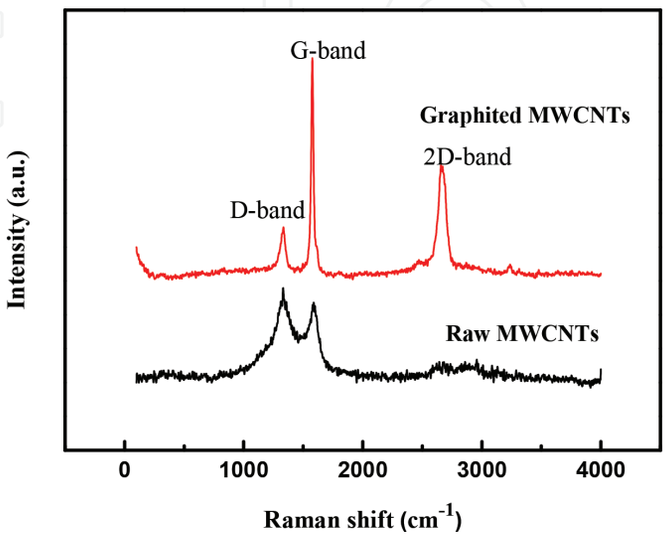

Figure 2. The Raman spectra of graphitization and raw MWCNTs.

http://dx.doi.org/10.5772/intechopen.79164

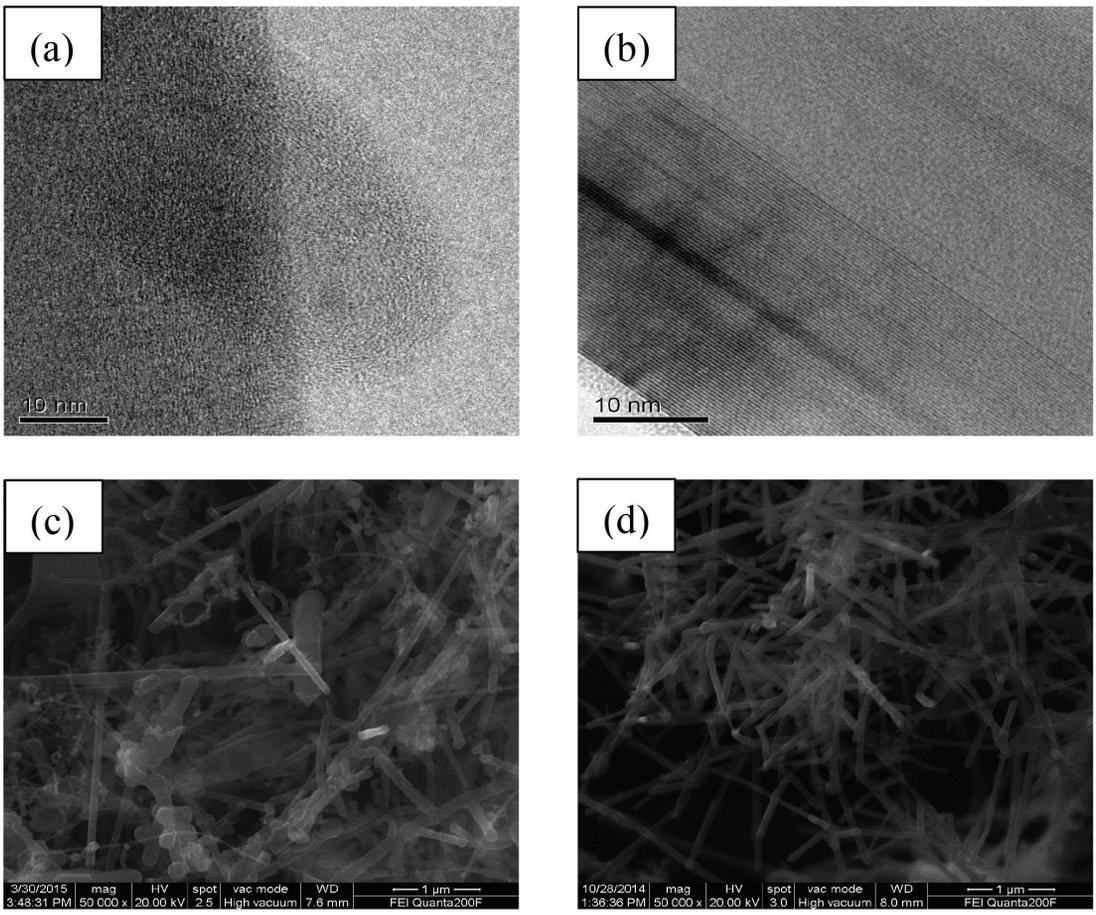

Figure 3. The TEM of R-MWCNTs (a), G-MWCNTs (b), the SEM of R-MWCNTs (c), and G-MWCNTs (d).

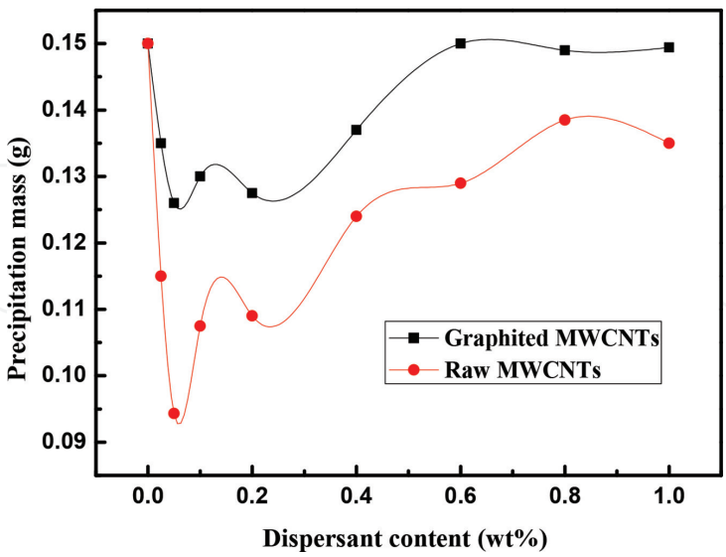

Figure 4. The precipitation mass of MWCNTs conducting liquids after centrifuged 10 min.

precipitation quality is around 0.0943 g with a dispersant of 0.05 wt.%. Van der Waals attraction between MWCNTs causes MWCNTs flocculation resulting in the formation of the aggregates and precipitation. The centrifugation treatment accelerated the sediment. The dispersant

can disperse the MWCNTs aggregates and form stable dispersion liquid of ethanol. When the dispersant content exceeded a critical value, the micelles of the dispersant are formed and resulted in the aggregation of MWCNTs and more precipitates.

In addition, the precipitation produced by G-MWCNTs conducting liquid after centrifugation is higher than that of R-MWCNTs conductive liquid as shown in **Figure 4**. This is owing to that R-MWCNTs absorbed the dispersant molecules on the surface which checked the aggregation of R-MWCNTs. However, graphitization eliminated the surface defects of G-MWCNTs, which reduces the adsorption of dispersant molecules on the surface. Therefore, the conductive liquid of G-MWCNTs is easier to precipitate than R-MWCNTs after centrifugation treatment.

3.2.3. Observation of MWCNTs conductive liquid

After 5 days of standing of R-MWCNTs dispersion, only the 1# shown obvious delamination and sediment phenomenon and other samples maintained unchanging (**Figure 5(a)**). **Figure 5(b)** shows the conductive liquid of G-MWCNTs. The 9#(0% dispersant), 13#(0.4%), 14#(0.6%), 15#(0.8%) and 16#(0.1%) demonstrated obvious delamination and sediment. The 10#, 11# and 12# hold unchanging. The results showed that the stability of conductive liquid of R-MWCNTs was better than that of G-MWCNTs. This is attributed that R-MWCNTs have a lot of surface defects and absorbed much functional groups as OH. In addition, the stability of dispersion with different dispersant TNADIS mass fractions was analyzed (9#, 13#, 14#, 15#, and 16#). The results demonstrated the aggregation and sediment were enhanced with increasing dispersant which surpass the critical concentration.

MWCNTs conductive liquid (3#) with 0.05 wt.% TNADIS showed excellent stability and no obvious sedimentation was observed after resting at room temperature for 5 months. When a beam of light passes through the colloid, a bright path in the colloid can be observed from the direction of the incident light. This phenomenon is called the Tyndall effect. The Tyndall effect of the conductive liquid of R-MWCNTs was examined before and after standing for 5 months. The optical path can be seen in the conductive liquid (**Figure 6**). It is shown that the conductive liquid of R-MWCNTs has a good stability and still remained colloidal properties after standing for 5 months.

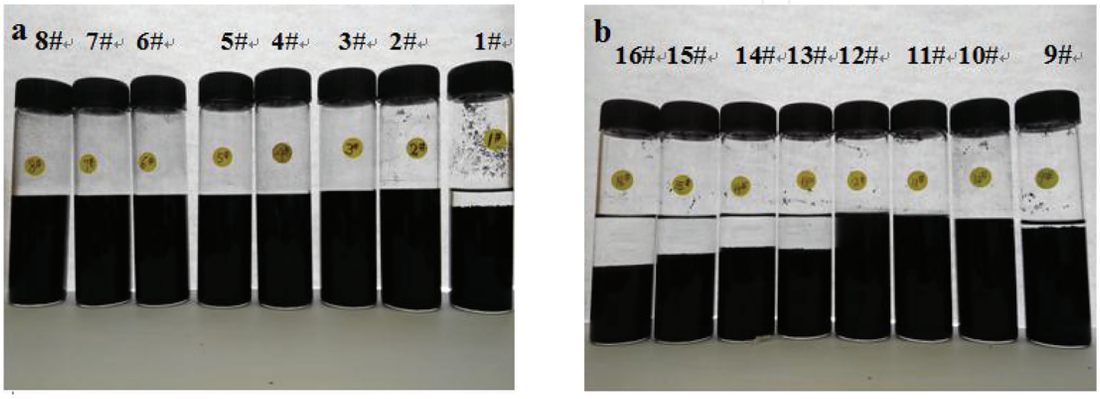

Figure 5. The raw (a) and graphitization (b) MWCNTs conducting liquid of stewing 5 days.

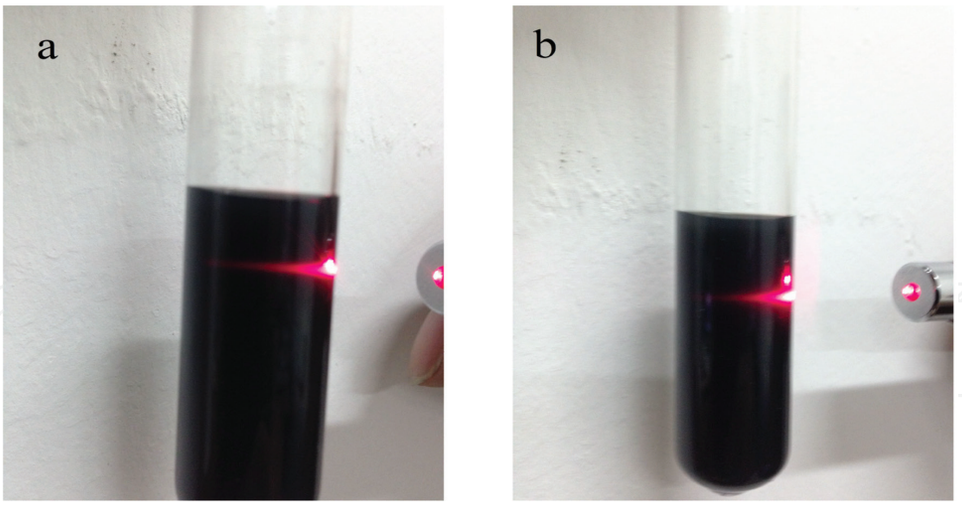

Figure 6. The Tyndall effect of R-MWCNTs conductive liquid before (a) and after (b) resting for 5 months.

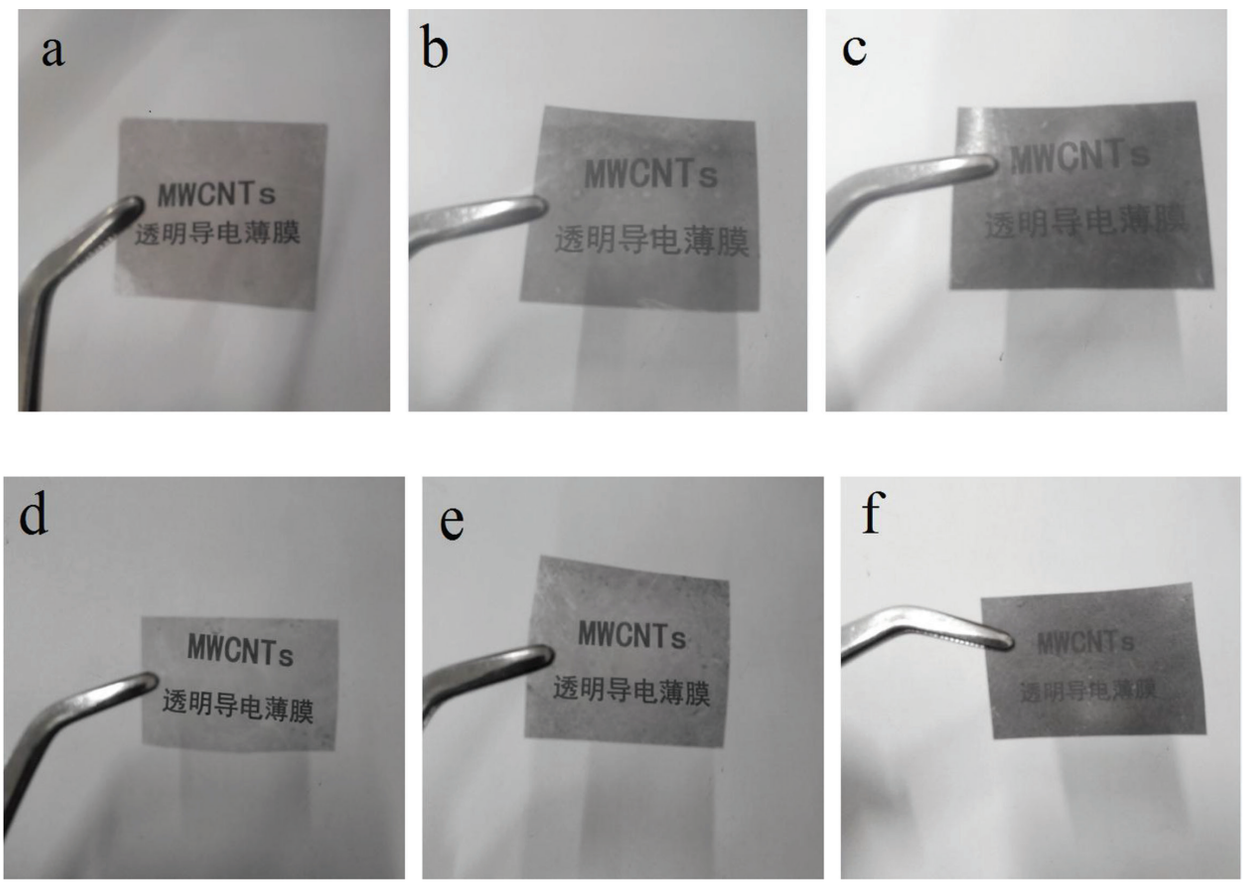

Figure 7. The R-MWCNTs (a, b, c) and G-MWCNTs (d, e, f) transparent conducting film.

3.2.4. Preparation and properties of MWCNTs transparent conductive film

The preparation method of MWCNTs transparent conductive films has high requirements on the dispersion properties of MWCNTs. The dispersion properties have a great influence on the film quality, electrical conductivity and transparency [34–41]. The 3#R-MWCNTs

The number of spin-coating		One	Twice	Three
R-MWCNTs	Square resistance kΩ/sq	103.3	10.6	3.7
	Transmittance (%)	68.3	57.9	52.8
G-MWCNTs	Square resistance kΩ/sq	53.6	2.8	0.34
	Transmittance (%)	68.9	58.1	53.3

Table 1. The square resistant and transmittance of MWCNTs transparent conducting film.

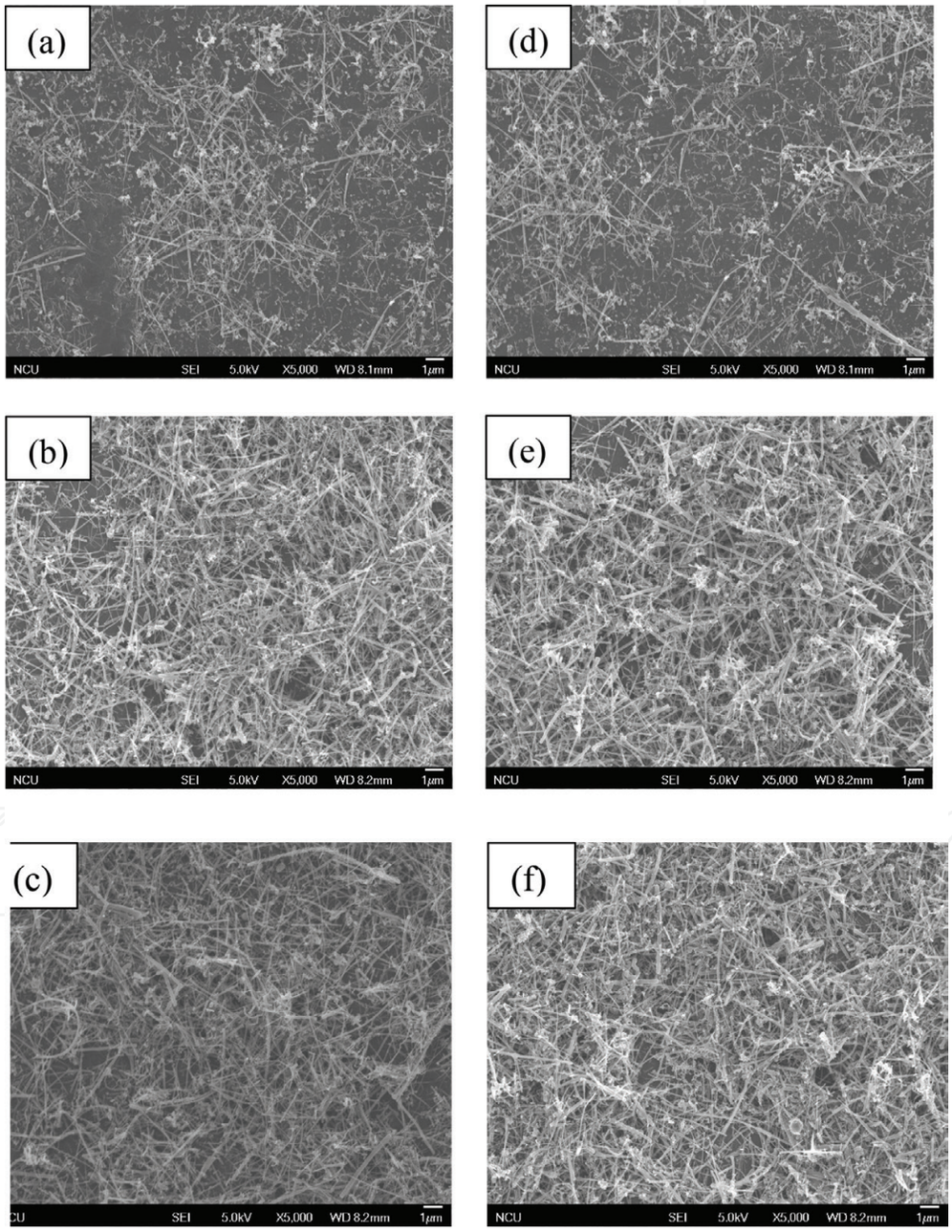

Figure 8. The SEM MWCNTs transparent conducting film. (a, b, c) R-MWCNTs spin-coating for once, twice, and thrice. (d, e, f) G-MWCNTs spin-coating for once, twice, and thrice.

conductive liquid and the 11#G-MWCNTs conductive liquid were applied onto the PET transparent film by spin-coating. The content of MWCNTs on the transparent film was controlled by controlling the number of spin-coating. After being spin-coated for once, twice, and thrice, respectively, the films were dried in vacuum drying oven. The square resistance of the dried MWCNTs transparent conductive film was measured with an ST-2258C multifunction digital four-probe tester.

Figure 7 shows spin-coated MWCNTs transparent conductive film. The transmittance of the film gradually decreases with increasing the number of spin-coating.

Compared with the resistance and transmittance of the R-MWCNTs and G-MWCNTs transparent conductive films, it was found that the transmittance of conductive films with the same number of spin-coating is almost the same. But, the conductivity of G-MWCNTs transparent conductive films was significantly better than that of R-MWCNTs as shown in **Table 1**. The main reason was that the G-MWCNTs obtained very high crystallinity and purity after high temperatures treatment of 3000°C. This resulted in higher electrical conductivity of G-MWCNTs transparent conductive films. In addition, as the number of spin-coating increases, the light transmittance of films gradually decreases and the conductivity increased.

Compared with the SEM image (**Figure 8**) of the conductive films, it was found that as the spin-on time increases, the MWCNTs gradually formed a continuous and dense mesh. The electronic transmission path was constructed, and the electrical conductivity was improved. After the spin-coating of G-MWCNTs conductive liquid for three times, the square resistance of the conductive film was 0.34 kΩ/sq.

4. MWCNTs transparent conducting film as interlayer for Li-S batteries

4.1. Experiment

4.1.1. Preparation of MWCNT paper collector

The MWCNT powder was dispersed in distilled water by sonication for 1 h and followed by high-speed shearing for 1 h with an addition of sodium dodecyl sulfate (SDS) as a surfactant. The cellulose fibers were prepared by smashing recycled papers in distilled water by high-speed shearing for 1 h. The MWCNT dispersion liquid and the cellulose fibers were mixed by high-shear emulsifier to form suspension for 2 h. The MWCNTs paper (MWCNTsP) was obtained by vacuum filtration through the suspension liquid of cellulose and MWCNTs. The MWCNTsP was rolled and tailored as current collector to host sulfur for cathodes.

4.1.2. Preparation of sulfur electrodes

Sulfur, MWCNTs and carbon black (CB) were mixed by balling for 1 h at 200 r/min. The slurry of sulfur was prepared by balling process with N-methyl-2-pyrrolidone (NMP) as solution

and PVDF as binder. The ratio of S : MWCNT : CB : PVDF = 60 : 15 : 15 : 10. The blend slurry was coated on to porous MWCNTsP. Then the sulfur electrodes (S-MWCNTsP) were dried at 60°C under vacuum for 12 h.

The conductive liquid of MWCNTs was prepared by ultrasonication and high-shear process with NMP as solution and PVDF as binder. The ratio of MWCNTs : CB : PVDF = 60 : 30 : 10. Subsequently followed by overlaying the conductive liquid onto S-MWCNTsP electrodes, the obtained electrode with MWCNTs transparent conducting film (TCF@S-MWCNTsP).

4.1.3. Assembling of cell and electrochemical measurements

The tailored S-MWCNTsP and TCF@S-MWCNTsP electrodes were, respectively, used as working electrodes. Lithium foil was used as the counter electrode and Celgard 2300 was used as the separator. The solution of 1.0 M LiTFSI in DOL:DME (1,1, vol.) with 1.0%LiNO3 was utilized as the electrolyte. CR2025 coin-type cells were assembled in an Ar filled glove box (MBRAUN LABSTAR, Germany). The electrochemical characterization of the cells was measured by a cell tester (CT-4008-5V5mA-164). The galvanostatic charge-discharge current density was set at 0.2 to 5C. Electrochemical impedance spectroscopy (EIS) and cyclic voltammetry (CV) within a potential window of 1.6–2.8 V by an electrochemical workstation (CHI 660B) were measured.

4.2. Results and discussion

4.2.1. The SEM of MWCNTsP and TCF@S-MWCNTsP electrode

Top surface SEM of the MWCNTsP in **Figure 9(a)** displays its porous matrix and the coalescing fiber network. The MWCNTsP demonstrated homogenous incorporation of MWCNTs in the cellulose fiber network. Porous structure can effectively improve the carrying capacity of sulfur, and adsorbed PSs. The superior electrolyte absorbability and hierarchical open channel of MWCNTsP can store more sulfur and contributes to stabilize electrochemical reactions and anchored PSs within the MWCNTsP effectively and suppressing shuttle effects. The SEM image of TCF@S-MWCNTsP electrode in **Figure 9(b)** also shows that MWCNTs and S were

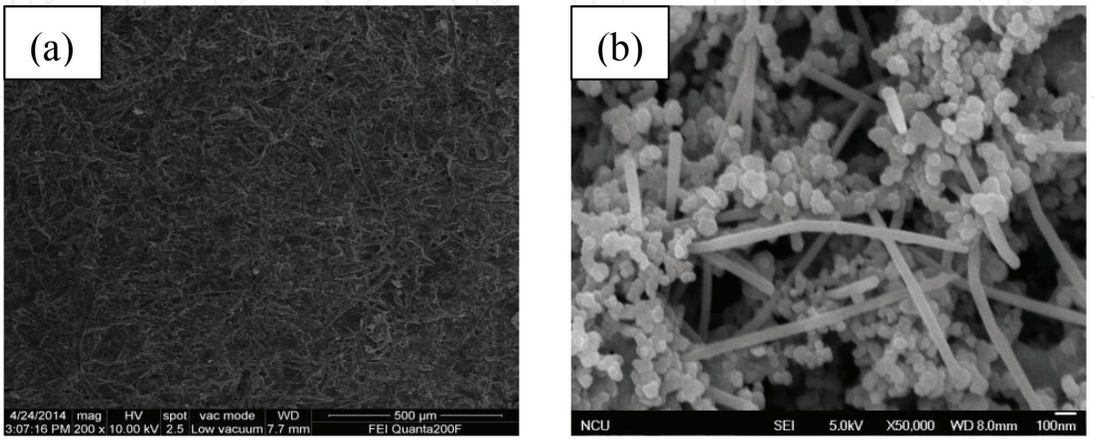

Figure 9. The SEM image of MWCNTsP (a) and TCF@S-MWCNTsP electrode (b).

dispersed evenly and well-connected, which should improve the conductivity of the electrodes and trapped more active material in its micropores toward the cathode side than that toward the anode side. The excellent electrolyte immersion and active material encapsulation also confirm the intimate connection between the insulating active material and the conductive matrix.

4.2.2. GTG of the TCF@S-MWCNTsP electrode

It can be indicated from **Figure 10** that the TCF@S-MWCNTsP electrode had a sulfur content of around 14 wt.% according to the main weight loss at T1 interval, which was attributed to sulfur sublimation. The weight loss at T2 interval which was attributed to carbonization of paper fibers. The weight of the electrode is 26 mg and is the average mass of the pole piece, and this can be calculated as the areal mass loading of sulfur in the cathode is 2.4 mg/cm^2.

4.2.3. Cyclic voltammetric characteristics

Cyclic voltammetry (CV) plots of the TCF@S-MWCNTsP electrode for the initial three cycles are shown in **Figure 11(a)**, recorded at a slow scan rate of 0.1 mV/s between 1.6 and 2.8 V. In the first electrode scan, two characteristic reduction peaks at 2.29 and 1.99 V can be observed, corresponding to the reduction of elemental sulfur (S_8) to long-chain PSs (Li_2S_n,4 ≤ n ≤ 8) and the subsequent formation of short-chain Li_2S_2/Li_2S, respectively. In the anodic sweep, two oxidation peaks are observed at 2.43 and 2.47 V, which owing to the conversion of short-chain to long-chain PSs, and the subsequent oxidization to S_8 [24, 42, 43].The third-cycle CV curve is highly similar to the second-cycle curve, thus it can be expected that the TCF@S-MWCNTsP electrode will show favorable cycling stability and high reversibility

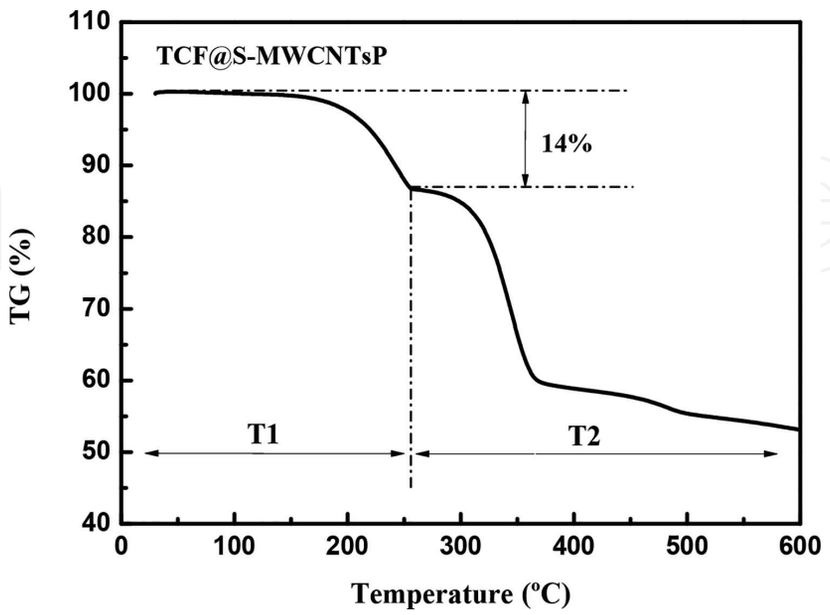

Figure 10. TG curve of the TCF@S-MWCNTsP electrode.

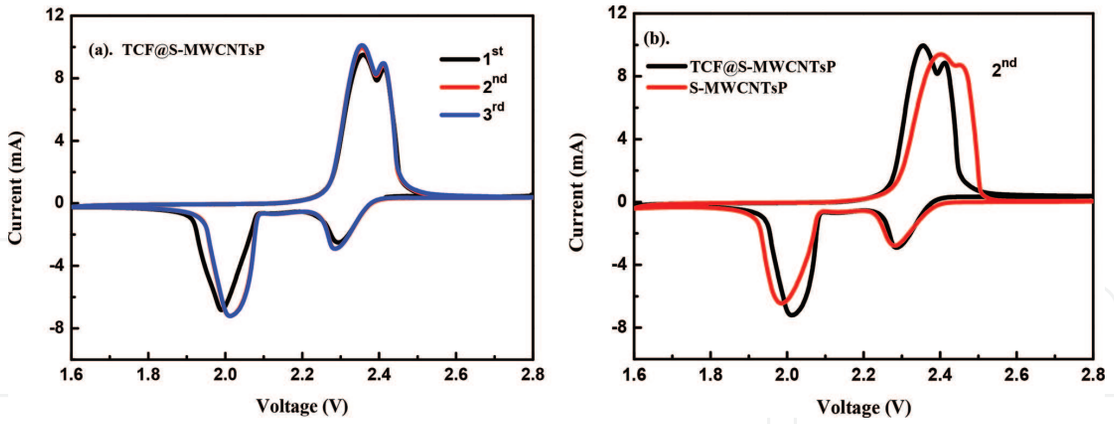

Figure 11. CV curves of Li-S batteries. (a) The first three cycles of CV profiles for TCF@S-MWCNTsP electrode. (b) The second cycle of CV profiles for TCF@S-MWCNTsP and S-MWCNTsP electrodes.

[44]. **Figure 11(b)** shows the second cycle of the CV plots for the two cathodes. There is a voltage shift between TCF@S-MWCNTs and S-MWCNTs electrodes other than the shape difference. This proves that using MWCNTsP as a current collector is beneficial to improve the electrochemical performance of a Li-S batteries. In addition, the TCF@S-MWCNTs electrode shows a higher voltage value at the reduction peaks and the oxidation peaks have a lower voltage value. This shows that the TCF@S-MWCNTs electrode has a higher discharge platform, which is conducive to improving the specific capacity and suppressing the shuttle effect. Meanwhile, the sharp reduction and oxidation peaks are also clear evidence of high reactivity of sulfur in the TCF@S-MWCNTs electrode. These results suggested that the electrode with MWCNTs transparent conducting film can inhibit effectively the shuttle effect and anchored PSs.

4.2.4. Constant current charge and discharge

Figure 12(a) shows the galvanostatic discharge–charge voltage profiles of S-MWCNTsP electrode at current rate 0.2 C (1 C = 1675 mAh/g) in the potential range from 1.6 to 2.8 V. It can be seen that there are two discharge plateaus for different rate at 2.3 and 2.1 V, respectively. But, only 2.1 V plateau exhibited a longer flat range which was ascribed to conformation of short-chain sulfides of Li_2S_2 and Li_2S. After 20 cycles, the discharge capacity also faded to 968 mAh/g from initial 1282 mAh/g. Another distinct characteristic is that Coulombic efficiency faded to 90.0% from initial 98.5%. It was considered the low Coulombic efficiency after 20 cycles was resulted from dissolution of long-chain PSs in electrolyte and subsequent migration and deposition on lithium anode. **Figure 12(b)** shows the galvanostatic discharge-charge voltage profiles of TCF@S-MWCNTsP electrode at current rate 0.2 C. The galvanostatic charge-discharge curves displayed a similar profile as S-MWCNTsP electrode. But, both the voltage plateaus of 2.3 and 2.1 V all exhibited longer flat range than ones of S-MWCNTsP electrode, indicating an excellent potential stability. The Coulombic efficiency and discharge capacity after 20 cycles reached 94.8% and 1028 mAh/g, respectively. This indicates that electrode with MWCNTs transparent conducting film can increase discharge capacity and Coulombic efficiency, inhibit shuttle effect.

http://dx.doi.org/10.5772/intechopen.79164

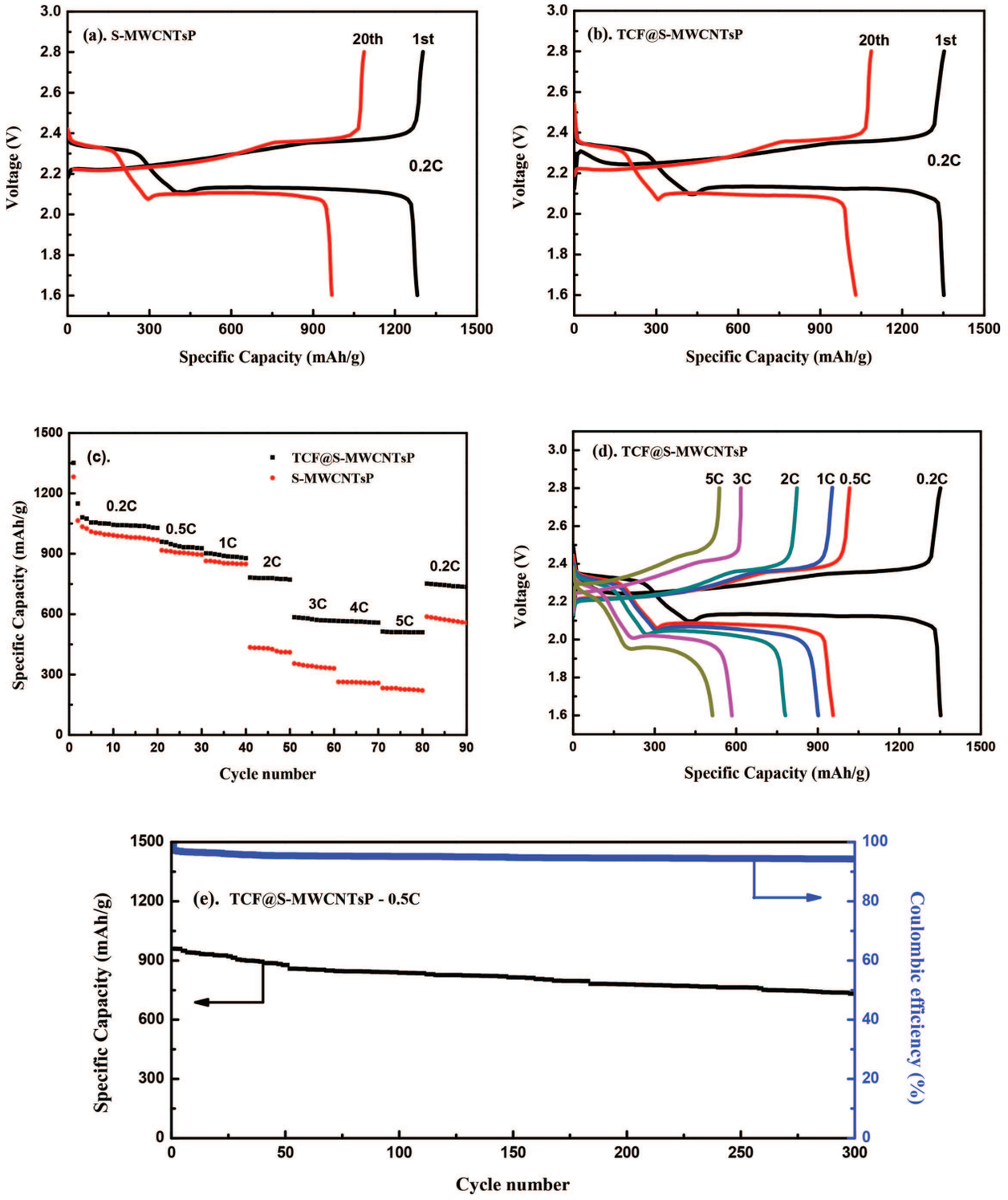

Figure 12. Electrochemical performance of Li-S batteries. Galvanostatic charge-discharge profiles of the (a) S-MWCNTsP and (b) TCF@S-MWCNTsP electrodes at 0.2 C. (c) The rate performance of TCF@S-MWCNTsP and S-MWCNTsP electrodes. (d) Galvanostatic charge-discharge profiles of the TCF@S-MWCNTsP electrode at various rates. (e) Long cycling performance of TCF@S-MWCNTsP electrode at 0.5 C.

Then the electrochemical performance of a Li-S cell was tested by galvanostatic discharge and charge from 1.6 to 2.8 V (versus Li/Li^+) at different current rates, and the areal mass loading of sulfur in the cathode is controlled to be approximately 2.4 mg/cm^2. **Figure 12(c)**

exhibits the rate performance of the two cathodes ranging from 0.2 to 5 C. Compared with the S-MWCNTsP and TCF@S-MWCNTsP cells, the TCF@S-MWCNTsP cell delivers a much higher initial capacity of 1352 mAh/g at the rate of 0.2 C, followed by a subsequent slow decrease to 960, 902, and 782 mAh/g at rates of 0.5, 1, and 2 C, respectively. In addition, at higher rates of 3 and 5 C, a reversible capacity of 584 and 513 mAh/g can still be achieved. When suddenly switching back to the initial starting rate of 0.2 C, the original capacity was recovered, indicating the excellent reversible capacity of the TCF@S-MWCNTsP cell at various rates. These results indicate that the electrode with MWCNTs transparent conducting film is conducive to immobilizing sulfur and alleviating the dissolution of polysulfides. The charge-discharge curves of the TCF@S-MWCNTsP electrode at various current rates (0.2–5 C) are illustrated in **Figure 12(d)**. All the discharge curves exhibit two typical plateaus, which are well consistent with the CV results. The charge-discharge voltage plateaus remain stable during the prolonged cycles, indicating an excellent potential stability. Additionally, the charge-discharge curves of the TCF@S-MWCNTsP electrode show also high Coulombic efficiency.

Long-term cycling stability with high-capacity retention is crucial for the practical application of Li − S batteries. **Figure 12(e)** shows the cycling performance of the TCF@S-MWCNTsP electrode at 0.5 C for 300 cycles. The electrode with MWCNTs transparent conducting film delivers a high initial reversible capacity of 960 mAh/g, and the capacity remains at 730 mAh/g after 300 cycles with stabilized coulombic efficiency above 94.2%, corresponding to a capacity retention of 76% and slow capacity decay rate of 0.08% per cycle. Additionally, the TCF@S-MWCNTsP electrode had the high Coulombic efficiency over 300 cycles, proving that the electrode with MWCNTs transparent conducting film can effectively suppress the notorious shuttle effect and improve the cycling stability.

4.2.5. Electrochemical impedance spectroscopy

The role of the electrode with MWCNTs transparent conducting film in Li-S batteries was further probed by electrochemical impedance spectroscopy (EIS). Nyquist plots of the two cells impedance before cycles are shown in **Figure 13(a)**. In the high-frequency region, the intercept of the impedance curve on the x-axis corresponds to the electrolyte resistance (Re). In the middle-frequency region, the semicircle arises from the charge transfer resistance (Rct), which represents the charge-transfer process at the interface between the electrolyte and electrode. In the low-frequency region, an inclined line denotes the Warburg resistance (Wo), which is related with mass transfer processes [45, 46]. The TCF@S-MWCNTsP electrode has the lower Rct value, indicating a low resistance caused by the entrapment of the dissolved PSs and both good electrolyte infiltration and charge transport. After 90 cycles, the Rct of S-MWCNTsP and TCF@S-MWCNTsP electrodes all demonstrates a decline as shown in **Figure 13(b)**. This can be ascribed to good electrolyte infiltration and the dramatic improvement of electronic and ionic conductivity due to the unique porous conductive interlinked structure of MWCNTsP. But the Re of both electrodes all demonstrates a rise. The increase of Re is caused by the dissolution and diffusion of PSs into the electrolyte. The lower Re value of the TCF@S-MWCNTsP electrode can be attributed to the use of the MWCNTs transparent conducting film framework can anchor PSs effectively and suppressing shuttle effects. Simultaneously, the electrode with

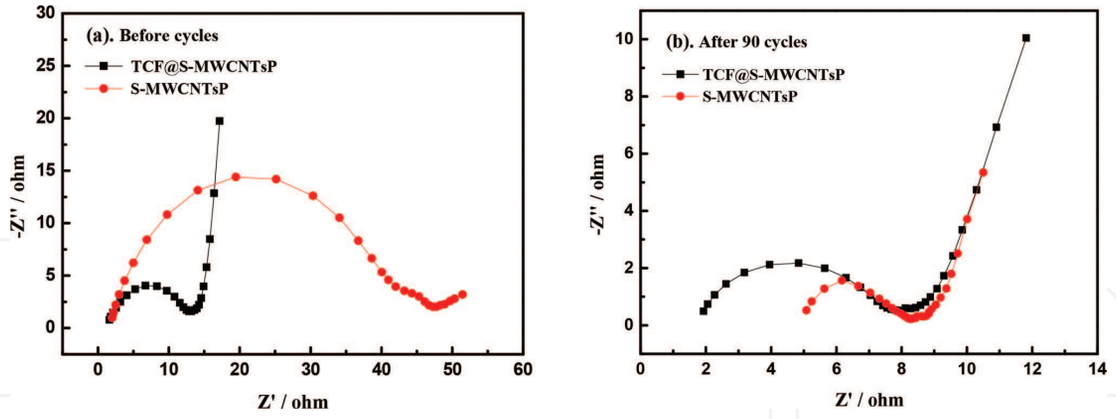

Figure 13. Electrochemical impedance spectroscopy of the two electrodes (a) before and (b) after cycles.

MWCNTs transparent conducting film could effectively reuse the dissolved active materials and mitigate surface aggregation, thus providing better performance.

5. Conclusions

The surface of R-MWCNTs has irregular arrangement of carbon atoms and much defects, which are more favorable for the adsorption of dispersant molecules. The dispersion effect and stability of R-MWCNTs are better than those of G-MWCNTs conductive fluids. With the increase of the dispersant TNADIS mass fraction, the dispersion effect of MWCNTs is getting better and better. When added to 0.05 wt.% dispersant, the dispersion effect of MWCNTs is best, and then the dispersive effect becomes worse as the dispersant TNADIS increases. With the increase of the quality of the dispersant TNADIS, the density of the MWCNTs precipitates becomes larger and larger, and the excess dispersant makes the MWCNTs agglomerate more and more closely. The conductivity of the conductive liquid with 0.05% dispersant was very high. After standing for 5 months, there was no obvious precipitation and the Tyndall effect of the colloid was still significantly maintained. Transparent conductive films prepared from conductive liquids of G-MWCNTs have better conductivity. After the three layers of spin-coating, the electrical conductivity of G-MWCNTs film surpassed three times than R-MWCNTs.

In summary, the designed electrode with MWCNTs transparent conducting film (TCF@S-MWCNTsP) showed significantly enhanced improvements in capacity retention and long-term cycle stability in Li − S batteries. The synergistic effect of them contributed to good rate performance, high capacity and excellent Coulombic efficiency. The areal sulfur mass loading of electrode is controlled to be above 2.4 mg/cm^2, a high discharge specific capacity of 1352 mAh/g can be delivered at 0.2 C with a Coulombic efficiency of 100%. Notably, the TCF@S-MWCNTsP electrode displayed a long cycling performance with only 0.08% capacity decay per cycle over 300 cycles at 0.5 C. The improved performance is ascribed to the trapping capability of the 3D configuration electrode to reutilize the dissolved polysulfides and the reduction of charge transfer impedance of the electrode. We believe that this attempt gives new insights on the cathode design for achieving high performance Li-S batteries.

Author details

Xiaogang Sun*, Jie Wang, Wei Chen, Xu Li, Manyuan Cai, Long Chen, Zhiwen Qiu, Yapan Huang, Chengcheng Wei, Hao Hu and Guodong Liang

*Address all correspondence to: xiaogangsun@163.com

Nanchang University, Nanchang, China

References

[1] Sheng L, Jin A, Yu L, et al. A simple and universal method for fabricating linear carbon chains in multiwalled carbon nanotubes. Materials Letters. 2012;**81**(3):222-224

[2] Ghosh K, Kumar M, Maruyama T, et al. Tailoring the field emission property of nitrogen-doped carbon nanotubes by controlling the graphitic/pyridinic substitution. Carbon. 2010;**48**(1):191-200

[3] Wang H, Li Z, Ghosh K, et al. Synthesis of double-walled carbon nanotube films and their field emission properties. Carbon. 2010;**48**(10):2882-2889

[4] Shinke K, Ando K, Koyama T, et al. Properties of various carbon nanomaterial surfaces in bilirubin adsorption. Colloids and Surfaces. B, Biointerfaces. 2010;**77**(1):18-21

[5] Ghosh K, Kumar M, Maruyama T, et al. Microstructural, electron-spectroscopic and field-emission studies of carbon nitride nanotubes grown from cage-like and linear carbon sources. Carbon. 2009;**47**:1565-1575

[6] Andoa K, Shinkea K, Yamadaa S, Koyamab T, et al. Fabrication of carbon nanotube sheets and their bilirubin adsorption capacity. Colloids and Surfaces. B, Biointerfaces. 2009;**71**(2):255-259

[7] Jiang X, Lu C, Song J, et al. Preparation of multi-walled carbon nanotubes acetone solution and study of dispersion stability. Insulating Materials. 2011;**44**(4):9-12

[8] Qi X. Dispersion of carbon nanotubes in aqueous solution with cationic surfactant CTAB. Journal of Inorganic Materials. 2007;**22**(6):1122-1126

[9] Kumar M, Ando Y. Camphor-a botanical precursor producing garden of carbon nanotubes. Diamond & Related Materials. 2003;**12**(5):998-1002

[10] Shimizu T, Abe H, Ando A, et al. Electric transport measurement of a multi-walled carbon nanotube in scanning transmission electron microscope. Physica E: Low-dimensional Systems and Nanostructures. 2004;**24**:37-41

[11] Taniguchi M, Nagao H, Hiramatsu M, et al. Preparation of dense carbon nanotube film using microwave plasma-enhanced chemical vapor deposition. Diamond & Related Materials. 2005;**14**(1):855-858

[12] Endo M, Takeuchi K, Hiraoka T, et al. Stacking nature of graphene layers in carbon nanotubes and nanofibres. Journal of Physics & Chemistry of Solids. 1997;**58**(11):1707-1712

[13] Endo M, Kim C, Karaki T, et al. Structural characterization of milled mesophase pitch-based carbon fibers. Carbon. 1998;**36**(11):1633-1641

[14] Endo M, Kim YA, Hayashi T, et al. Microstructural changes induced in "stacked cup" carbon nanofibers by heat treatment. Carbon. 2003;**41**(7):1941-1947

[15] Wakiwaka H, Kodani M, Endo M, et al. Non-contact measurement of CNT compounding ratio in composite material by eddy current method. Sensors & Actuators A Physical. 2006;**129**(1):235-238

[16] Xie JL, Chen XY, Jin H, et al. Synthesis and characterization of stable graphene colloidal dispersions. Journal of Functional Materials. 2014;**45**(12):12108-12112

[17] Ma P, Siddiqui NA, Marom G, et al. Dispersion and functionalization of carbon nanotubes for polymer-based nanocomposites: A review. Composites Part A Applied Science & Manufacturing. 2010;**41**(10):1345-1367

[18] Gauthier M, Reyter D, Mazouzi D, et al. From Si wafers to cheap and efficient Si electrodes for Li-ion batteries. Journal of Power Sources. 2014;**256**(12):32-36

[19] Yang Y, Zheng G, Cui Y. Nanostructured sulfur cathodes. Chemical Society Reviews. 2013;**42**(7):3018-3032

[20] Liang J, Sun ZH, Li F, et al. Carbon materials for Li–S batteries: Functional evolution and performance improvement. Energy Storage Materials. 2016;**2**:76-106

[21] Manthiram A, Fu Y, Chung SH, et al. Rechargeable lithium-sulfur batteries. Chemical Reviews. 2014;**114**(23):11751

[22] Evers S, Nazar LF. New approaches for high energy density lithium–sulfur battery cathodes. Accounts of Chemical Research. 2013;**46**(5):1135

[23] Sen X et al. Smaller sulfur molecules promise better lithium–sulfur batteries. Journal of the American Chemical Society. 2012;**134**(45):18510-18513

[24] Yu M, Ma J, Song H, et al. Atomic layer deposited TiO_2 on a nitrogen-doped graphene/sulfur electrode for high performance lithium–sulfur batteries. Energy & Environmental Science. 2016;**9**(4):1495-1503

[25] Zhang Q, Wang Y, Zhi WS, et al. Understanding the anchoring effect of two-dimensional layered materials for lithium–sulfur batteries. Nano Letters. 2015;**15**(6):3780

[26] Manthiram A, Chung SH, Zu C. Lithium-sulfur batteries: Progress and prospects. Advanced Materials. 2015;**27**(12):1980-2006

[27] Pang Q, Kundu D, Cuisinier M, et al. Surface-enhanced redox chemistry of polysulphides on a metallic and polar host for lithium-sulphur batteries. Nature Communications. 2014;**5**:4759

[28] Mikhaylik YV, Akridge JR. Polysulfide shuttle study in the Li/S battery system. Journal of the Electrochemical Society. 2004;**151**(151):A1969-A1976

[29] Busche MR, Adelhelm P, Sommer H, et al. Systematical electrochemical study on the parasitic shuttle-effect inlithium-sulfur-cells at different temperatures and different rates. Journal of Power Sources. 2014;**259**:289-299

[30] Zhang J, Hu H, Li Z, et al. Double-shelled nanocages with cobalt hydroxide inner shell and layered double hydroxides outer shell as high-efficiency polysulfide mediator for lithium-sulfur batteries. Angewandte Chemie. 2016;**55**(12):3982

[31] Hofmann AF, Fronczek DN, Bessler WG. Mechanistic modeling of polysulfide shuttle and capacity loss in lithium–sulfur batteries. Journal of Power Sources. 2014;**259**(259):300-310

[32] Zhou G, Pei S, Li L, et al. A graphene–pure-sulfur sandwich structure for ultrafast, long-life lithium–sulfur batteries. Advanced Materials. 2014;**26**(4):625-631

[33] Huang JQ, Zhang Q, Wei F. Multi-functional separator/interlayer system for high-stable lithium-sulfur batteries: Progress and prospects. Energy Storage Materials. 2015;**1**:127-145

[34] Ko W, Su J, Guo C, et al. Highly conductive, transparent flexible films based on open rings of multi-walled carbon nanotubes. Thin Solid Films. 2011;**519**(22):7717-7722

[35] Shin E, Jeong G. Fabrication of transparent, flexible and conductive films using as-grown few-walled carbon nanotubes. Current Applied Physics. 2011;**11**(4):S73-S77

[36] Xiao G, Tao Y, Lu J, et al. Highly conductive and transparent carbon nanotube composite thin films deposited on polyethylene terephthalate solution dipping. Thin Solid Films. 2010;**518**(10):2822-2824

[37] Jung R, Kim H, Kim Y, et al. Electrically conductive transparent papers using multiwalled carbon nanotubes. Journal of Polymer Science Part B Polymer Physics. 2008;**46**(12):1235-1242

[38] Jo S, Lee Y, Yang J, et al. Carbon nanotube-based flexible transparent electrode films hybridized with self-assembling PEDOT. Synthetic Metals. 2012;**162**(13-14):1279-1284

[39] Zhang J, Wen X, Song Q, et al. Research advances in fabrication technologies of transparent conducting carbon nanotube films. Materials Review. 2011;**25**(5):124-129

[40] Ning J, Zhi LJ. Advances in flexible transparent conductive films based on carbon nanomaterials. Chinese Science Bulletin. 2014;**59**:3313-3321

[41] SH L, CC T, CC M, et al. Highly transparent and conductive thin films fabricated with nano-silver/double-walled carbon nanotube composites. Journal of Colloid and Interface Science. 2011;**364**(1):1-9

[42] Zhao MQ, Zhang Q, Huang JQ, et al. Unstacked double-layer templated graphene for high-rate lithium-sulphur batteries. Nature Communications. 2014;**5**(5):3410

[43] Salem HA, Babu G, Rao CV, et al. Electrocatalytic polysulfide traps for controlling redox shuttle process of Li–S batteries. Journal of the American Chemical Society. 2015;**137**(36):11542

[44] Yijuan L et al. A honeycomb-like Co@N–C composite for ultrahigh sulfur loading Li–S batteries. ACS Nano. 2017;**11**(11):11417-11424

[45] Tao H, Mukoyama D, Nara H, et al. Electrochemical impedance spectroscopy analysis for lithium-ion battery using $Li_4Ti_5O_{12}$ anode. Journal of Power Sources. 2013;**222**(2):442-447

[46] Li S, Ren G, Hoque MNF, et al. Carbonized cellulose paper as an effective interlayer in lithium-sulfur batteries. Applied Surface Science. 2017;**396**:637-643

IntechOpen